Nat. Hazards Earth Syst. Sci. Discuss., 1, 7667–7700, 2013
www.nat-hazards-earth-syst-sci-discuss.net/1/7667/2013/
doi:10.5194/nhessd-1-7667-2013

Natural Hazards and Earth System Sciences
Open Access
Discussions

Ejection mechanism of the Donghekou landslide triggered by the 2008 Wenchuan Earthquake revealed by discrete element modeling

R.-M. Yuan[1,2], C.-L. Tang[3], J.-C. Hu[3], and X.-W. Xu[1]

[1]Key Laboratory of Active Tectonics and Volcano, China Earthquake Administration, Beijing, 100029, China
[2]Institute of Geology, China Earthquake Administration, Beijing, 100029, China
[3]Department of Geosciences, National Taiwan University, Taipei, 10617, Taiwan

Received: 24 August 2013 – Accepted: 29 October 2013 – Published: 23 December 2013

Correspondence to: J.-C. Hu (jchu@ntu.edu.tw)

Published by Copernicus Publications on behalf of the European Geosciences Union.

Abstract

The huge Donghekou landslide was triggered by the Wenchuan earthquake in 2008 with about 2.4×10^7 m^3 of rock displaced. The landslide is considered as an example of earthquake-induced ejection event, but the kinematic processes are not well understood. We used the 2-D granular discrete element method to characterize the kinematic behavior and mechanics of this ejection landslide. The initial boundary conditions were applied along the ball-wall contacts by using derived velocities integrated from strong motion data with a duration of 125 s, including the peak acceleration near the Donghekou area. The constraints were primarily determined from the final geometry of the landslide and geological structures to account for the actual landslide characteristics. Simulated results showed that the large local seismic acceleration and a free face under the sliding body, caused by the dip difference between the upper slide face and the natural slope, originated from the ejection of the landslide. For the lower slide body, its kinematic mechanism was changed during sliding. Initially it was a pushed landslide, and then gradually changed to a retrogressive landslide. The eroded bed on the slope during the landslide could slightly increase the runout distance from 1435 m to 1519 m, and was predicted in the numerical simulation.

1 Introduction

Earthquakes cause large-scale ground movement (shaking) and can trigger severe landslides over broad areas resulting in serious damage and casualties (Harp and Jibson, 1996; Central Geological Survey, 2000; Chigira et al., 2003; Keefer et al., 2006; Keefer and Larsen, 2007; Dai et al., 2010). To analyze an earthquake-induced landslide hazard, in addition to describing the regional correlation between seismic events and landslides under various conditions, it is critical to study the failure mechanism of catastrophic earthquake-induced landslides. However, the assessment of catastrophic landslides requires knowledge of landslide characteristics and runout mechanics.

The complex kinematics of the flowing mass depends on the morphological and geological characteristics of the slope, rheology of the surface material, and the triggering process. To better evaluate the failure mechanism within the moving mass and possible causes of the runout, both empirical and numerical models can be used. In general, empirical models lack robustness due to the comprehensive description of complex geological and geotechnical conditions of large flow-like landslides (e.g., Legros, 2002). However, a continuous method demonstrates the advantage of representing a complex geometry of a rock avalanche (Crosta et al., 2006). Refined numerical solutions and a Coulomb-like behavior have been successfully derived for landslides (Iverson and Denlinger, 2001; Iverson and Vallance, 2001; Denlinger and Iverson, 2004), which often involve heterogeneous granular materials such as rocks and debris that may fall, topple or slide (Cruden and Varnes, 1996). For numerical models, many researchers have adopted discrete-element methods to analyze landslides (Campbell et al., 1995; Poisel and Roth, 2004; Poisel et al., 2005; Staron, 2007; Peng, 2008; Tang et al., 2009a, b, 2012, 2013). This research validated numerical modeling based on discrete-element methods, which is a powerful tool for modeling rock slope susceptibility to earthquakes.

After the Donghekou landslide triggered by the 2008 Wenchuan Earthquake, several field investigations were carried out for landslide mapping and triggering mechanisms (Yin, 2008, 2009; Yin et al., 2009, 2011; Sun et al., 2009a, b; Wang et al., 2009; Tang et al., 2010; Yuan et al., 2010, 2013; Zhang et al., 2011; Huang and Fan, 2013). Meanwhile, numerical simulations based on various investigations were also applied to analyze the movement processes (Li et al., 2012; Zhang et al., 2012). However, the kinematic processes controlling the moving mass and the mechanism for some special phenomena associated with this huge landslide are still poorly understood because of the complicated movement processes and unique type.

In this paper, we try to address some special phenomena of the Donghekou landslide using the 2-D discrete element method for granular materials, which is helpful for characterizing the complex kinematics and triggering process of a large landslide.

We focus especially on explaining the ejection of the upper landslide body and the formation of two disconnected landslide surfaces.

2 The Donghekou landslide

On 12 May 2008, the M_w = 7.9 Wenchuan earthquake struck the Longmenshan area, Sichuan Province, China, along the middle segment of the Longmenshan thrust belt, at the eastern margin of the Tibetan Plateau (Fig. 1a). Field investigations showed that the co-seismic surface rupture zones along the Beichuan-Yingxiu fault and the Pengguan fault propagated unilaterally toward a northeast direction for over 300 km, involving thrusting and right lateral components (Xu et al., 2009).

The Wenchuan earthquake triggered thousands of mass movements in the Longmenshan area (Dai et al., 2010) where some huge landslides caused an extreme loss of life and property (Yin, 2008). Among these landslides, the Donghekou landslide was quite special, located at the northeast end of the Beichuan rupture (32.40572° N, 105.11081° E) and caused serious loss of life at the village of Donghekou, Qinchuan, Sichuan Province (Fig. 1a and b). It can be described as the combination of two effects: the primary landslide and a significant rock fall. In this paper, only the primary landslide is simulated to better understand its formation mechanism.

The primary landslide, with an estimated volume of about 2.4×10^7 m^3, originated at an elevation ranging between 1150 and 1350 m; it traveled downhill toward the northeast for about 2.45 km, and ended at the confluence of the Qingzhu and Hongshihe Rivers where two large lakes were formed. The vertical drop from the ridge to the rivers is approximately 600 m (Figs. 1b and 2).

The field investigation along profile A-B-C (position shown in Fig. 1b) reveals that the sliding surface is neither continuous nor uniform. Instead, the surface can be divided into two parts (Fig. 2): the upper, very rough and deep sliding face, and the lower, very shallow sliding surface. The upper sliding body cuts through the mountain top with a quite rough and steep main scarp, and one undisturbed ground area exists between

the upper and lower sliding surface. Therefore, it was inferred that the landslide started with material ejection due to the large local seismic acceleration, throwing rocks into the air with a parabolic trajectory before they fell back to the ground (Huang, 2009; Yuan et al., 2010; Xu and Dong, 2011; Zhang et al., 2011). A simple tectonic geomorphology model was introduced to explain the ejection phenomenon of the landslide (Yuan et al., 2010; Tang et al., 2010), but its complex kinematics and triggering process still remain poorly understood.

3 Geological setting of the Donghekou area

The Donghekou landslide is located in a mountainous region at the northern termination of the Beichuan rupture zone (Fig. 1). The elevation of the Dapingshan Mountain, where the Donghekou ejection landslide occurred, is 1609.6 m. Its slope is approximately uniform at 40°, though portions of the mountain surface are as steep as 70–80°. Such steep conditions are partly responsible for the occurrence of such a complex landslide.

The two main outcropping geological formations along the mountain slopes are dolomite limestone and siliceous phyllite. The dolomite limestone, with an occurrence of 139°/41°/26°, was observed mostly in the rock fall area, on the northwest side of the ejection landslide, and only a few limestone outcrops were found at the top of the slope (Fig. 2). In contrast, the siliceous phyllite, with an occurrence of 135°/45°/25°, was observed mainly in the area of the main landslide and in the zone of the domino-like ground tension fissures.

4 The Newmark displacement method and two-dimensional distinct element modeling

The Newmark displacement method and a discrete granular simulation technique were used in this paper to investigate the mechanics of the Donghekou landslide. The major

methodological and technical aspects of the numerical simulation are summarized below.

4.1 Principles of the Newmark displacement method

In 1965, N. M. Newmark first proposed the basic elements of a procedure for evaluating potential deformations of an embankment dam due to earthquake shaking (Newmark, 1965). By computing the ground motion acceleration at which the inertial force becomes sufficiently high to cause yielding, as shown in Fig. 3, and integrating the acceleration exceeding the yield acceleration in the sliding mass, the ultimate displacement can be evaluated. Here the authors applied the Newmark displacement method to calculate the free-body force of the Donghekou landslide mass during the 2008 Wenchuan earthquake, assuming that the block slid when the peak acceleration was beyond the yield acceleration. The free-body diagram illustrates the situation of the sliding block before the earthquake (Fig. 3). Thus the force normal to the slope is $mg\cos\delta$, where m is the mass of the free-body, g is the gravitational acceleration, and δ is the dip angle of the inclined surface. A basal friction force $\mu_s mg\cos\delta$ consequently balances the $mg\sin\delta$ downslope force generated by gravity, so that the stability condition can be written:

$$mg\sin\delta < \mu_s mg\cos\delta + cA, \tag{1}$$

where, μ_s is the coefficient of static friction, c is the cohesive strength along the sliding surface, and A is the area of the sliding surface.

We then introduced the safety factor, FS (Newmark, 1965; Wilson and Keefer, 1983) to evaluate the sliding threshold across an existing bedding plane:

$$\mathrm{FS} = \frac{\mu_s mg\cos\delta + cA}{mg\sin\delta} \tag{2}$$

For the Donghekou landslide, because the initial slide direction almost coincided with the dip of the underlying surface, the initial movement was inferred to be a nearly

pure translation. We adopted the cohesion of intact shale of $1.65 \times 10^4\,\mathrm{N\,m^{-2}}$ (Sun et al., 2009a), a density of $2.6\,\mathrm{g\,cm^{-3}}$ and a dip $\delta = 25^\circ$. The calculated FS was greater than 1. We inferred that sliding over an existing bedding plane is only possible if other external triggering mechanisms are present (such as an earthquake or rainfall), or if the down-dip acceleration a_d is beyond the yield acceleration.

To calculate the down-dip sliding acceleration, S, the data obtained from the nearest station measuring PGA (peak ground acceleration), situated in the Jiangyou valley at (31.8° N, 104.7° E), was used to analyze the PGA values in the Donghekou area:

$$S = (g\sin\delta - a_\mathrm{d}) - \mu_\mathrm{s}(g\cos\delta + a_\mathrm{n}) - cA/m \tag{3}$$

where a_d and a_n refer to the down-dip and normal-to-sliding components of acceleration, respectively.

4.2 Distinct element modeling

The technique of distinct element modeling (DEM) was first developed to simulate rock-block systems (Cundall, 1971); it was later applied to the modeling of granular material (Cundall and Strack, 1979). DEM is currently widely used in research related to rock mechanics and brittle tectonics (e.g., Hu and Angelier, 2004; Egholm, 2007; Egholm et al., 2007). The main calculation uses a time explicit method and is capable of bonding particles into a mass by bonds. PFC models are made up of discrete particles, allowing for individual movements. The points where particles touch each other are called contacts. The numerical modeling technique that we adopted for the experiments reported here involved a particular application, PFC2D, of the 2-D particle flow code (Itasca, 2002). This technique is commonly used for modeling granular assemblages with purely frictional or bonded circular particles represented by discs and is now widely used to resolve rock engineering and geo-mechanics problems (e.g., Wang et al., 2003; Potyondy and Cundall, 2004; Tang et al., 2009a, b, 2012, 2013).

4.2.1 Micro-properties

All numerical simulations by PFC modeling require proper selection of micro-parameters by means of calibration processes in which the response of the numerical modeling is compared with the observed results of the physical material. Attempts to improve and simplify the calibration process and modeling procedure have been reported in the literature (e.g., Itasca, 2002; Potyondy and Cundall, 2004). More recently, the application of experimental design and optimization in uniaxial compression simulations was proposed to calculate proper micro-parameters for model generation in PFC (Yoon, 2007). For a bond model, the overall mechanical behaviors of the assembly of particles are controlled by micro-properties such as normal and shear stiffness, normal and shear bonds, and the Coulomb friction coefficient. There is no straightforward solution with regard to micro-properties and macro-properties, but a relationship exists between the two scales of properties for an initial calibration.

Young's modulus of the material is linearly related to the value of contact stiffness. Parallel bonds increase contact stiffness (Itasca, 2002). Young's moduli of the grains (E_c) and cement ($\overline{E_\mathrm{c}}$) are expressed by:

$$E_\mathrm{c} = \begin{cases} \frac{k_n}{2t} & \text{, PFC2D Disk mode} \\ \frac{k_n}{4R} & \text{, PFC3D, PFC2D Sphere model} \end{cases} \tag{4}$$

$$\overline{E_\mathrm{c}} = k^P\left(R^{(A)} + R^{(E)}\right) \tag{5}$$

where, k_n, k^P, R and t are normal particle stiffness, parallel bond normal stiffness, particle radius, and disk thickness, respectively (Potyondy and Cundall, 2004). Thus, Poisson's ratio depends both on the ratio of shear contact stiffness to normal contact stiffness and packing geometry. The peak strength of the material depends both upon the friction coefficient and the bond strength (Itasca, 2002).

When using discrete element methods, the macroscopic behavior of the granular media depends on the contact mechanical micro-properties. Because there is no

straightforward method of linking microscopic and macroscopic parameters, a series of biaxial numerical tests were performed on granular samples to derive the mechanical macro-properties of the granular rock assembly. Because no complete theory can reliably predict macroscopic behavior from microscopic properties and geometry, the iterative trial-and-error processes in numerical biaxial tests were performed for the calibration of mechanical parameters. After parameter calibration, the micro-properties were used for the 2-D particle assembly in PFC, and are listed in Table 1.

4.2.2 Numerical model for the Donghekou landslide

The dimensions of the Donghekou landslide model were 2450 m in length and 750 m in height (Fig. 2). A profile of the slope was first built to perform a numerical simulation. In the numerical model, the rocks under the sliding surface were represented by "wall elements". Then, the particles composing the sliding mass were randomly generated inside the entire deforming region, including the upper sliding body and lower sliding mass (Fig. 4a). The different colors in the upper sliding body show the process of destroying the sliding body, and do not indicate different materials. To illustrate the velocity and displacement during sliding, some monitoring disks were installed within the upper and lower sliding blocks, as shown in Fig. 4b and c. The monitoring disks for the upper ejection body were chosen at different heights from the lower to the upper part. For the lower sliding body, the monitoring disks were chosen based upon the sliding face and ground surface.

The mechanical and geometrical properties of the elements are evaluated according to geological considerations. Based on in situ observations in the landslide area, the adopted disk diameter ranged from 1.28 to 2.56 m with a uniform distribution. Using these choices, the total number of particles was 10 000 for the upper and 5000 for the lower sliding bodies respectively. The inter-particle coefficient of friction was set at 0.5, which was determined from the residual friction coefficient of joints in the rock mass (Table 1). Strong motion vibration was applied to the model boundary by integrating the acceleration of the seismic station in the Jiangyou valley that recorded

the Wenchuan earthquake (Fig. 5a). Based on the data from this station and the scaling-up of the topography effect in this area suggested by Wang et al. (2009), the vertical and horizontal components along the slip direction of the Donghekou landslide were calculated (Fig. 5b).

In our series of experiments, we adopted variable values for two major parameters of the numerical experiments: the residual friction coefficient at the landslide surface and the internal bonding strength parameters. In the present paper, the residual friction coefficient ranged from 0.05 to 0.3, and two different values (50 and 10 MPa) were used for parallel bond strength. All the parameters used in simulation are listed in Table 1.

5 Results and analysis

During calculation and modeling, particular attention was devoted to displacement amplitudes and the sliding process, to analyze the failure mechanism and formation processes of the two separated landslide bodies of the Donghekou landslide.

5.1 Displacement amplitudes

The displacement and down-dip sliding acceleration of monitoring disks during the vibrations were calculated and simulated during the shaking process. We used the Newmark displacement method to analyze the acceleration of the Jiangyou station (see also Fig. 5). By integrating the effective acceleration on the sliding mass in excess of this yield acceleration as a function of time, velocities and ultimately displacements of the sliding mass were evaluated.

The calculations were based on three points with different local slopes, respectively, including points 4, 10 and 30 (Fig. 4); the friction coefficient was set at 0.5. When the acceleration reached the peak value, sliding was triggered. Point 4 was unstable, because the local slope was 39° ($\tan 39^\circ > 0.5$), allowing the rock mass to slide without earthquake action. For points 10 and 30, the calculations showed that several different

acceleration peaks existed beyond the yield acceleration (Fig. 6). Obvious deformation of slide block occurred at about 17 s and the landslide yielded thoroughly at about 35 s. After calculating the final integration of the peaks, we found a total sliding value between block and sliding surface, as determined by the Newmark displacement method, of about 311 cm for point 10 (Fig. 6: a-1) and about 31 cm for point 30 (Fig. 6: b-1).

If the influence of pore or fissure water on the landslide was not accounted for, the disks then only slid by no more than 311 cm for point 10 and 31 cm for point 30 during the Wenchuan earthquake, prior to the catastrophic event. The possible mechanisms of the Donghekou landslide will be discussed based on discrete particle simulations. At this stage, we show only the simulation results for these three points for comparison with the calculated results.

For the Donghekou landslide, the simulated displacements of disks 10, 30 and 4 during the seismic shaking process were calculated using a coefficient of friction of 0.5 (Fig. 6: a-2, b-2, c). In our simulation results, obvious deformation of the sliding block also occurred at about 17 s, and the landslide also yielded completely at about 35 s, which agreed with the values obtained from the Newmark displacement method. However, for the simulated displacements, the disks slid by no more than 672 cm for point 10, 926 cm for point 30 and 648 cm for point 4 during the Wenchuan earthquake, respectively, which obviously do not agree with the values obtained from Newmark displacement analysis. After the vibration simulation, the discordant shear displacement on the landslide detachment plane was observed. These gaps could be explained by the effect of interaction of particles included in the simulation method, such as collision between different disks (Tang et al., 2012). The upper part of the block collided down the lower part of the block, so the upper part of the block collided back by the lower part of the block. Hence, the displacement of the monitored point 30 is larger than those of monitored particles 4 and 10. In the Newmark method, only the movement of a single disk was calculated.

5.2 Sliding process

Because PFC2D uses an explicit solution scheme that gives stable solutions to unstable processes, it describes and accurately locates the non-linear behavior observed in the Donghekou landslide. Simulated results at different time steps can therefore be shown and described. The simulated results are shown in Fig. 7 and indicate that in the initial stage, the deformation only occurred in the upper sliding mass. Then, the upper sliding face was formed at about 35 s when the sliding body began to move down to gouge out the upper sliding base (Fig. 7b). Following that, the sliding body then collided with the ground at about 55 s, causing the lower sliding mass to slide (Fig. 7c). At 90 s, the lower sliding face was formed; the lower sliding mass also began to move down because of its weight and the thrusting of the upper sliding body (Fig. 7d). Thereafter, the landside arrived at the Qinzhujiang River at 120 s (Fig. 7e). In the final stage, the Qinzhujiang and Hongshihe rivers were cut off by the deposits of the landslide forming two lakes (Fig. 7f).

5.3 Runout distance

To illustrate the runout distances, some monitoring disks were incorporated into the sliding blocks (Fig. 4b and c). Every monitoring disk is assigned a number to identify the position change. Different colors are also used for the disks in different segments of the sliding block to facilitate discussion of deformation in the upper sliding block (Fig. 8a).

For the upper and lower sliding blocks, the initial lengths are about 300 m from monitoring disks 1 through 35, and about 500 m from monitoring disks 36 through 43, respectively. The entire length of the deposit area is about 1200 m. During sliding, the disks in the downslope area collided with the disks in the rear which underwent acceleration in the downslope direction. The runout distances of disks from the upper layers generally have longer runout distances than those from the deeper layers (Fig. 8b, Table 2). The disks in the lower sliding block formed a disordered pattern

because of collision or being shoveled by the upper slide block. Disk 36 in this block has a longer runout distance of about 1650 m, which is larger than that of disk 40. However, for the upper sliding body, the relative locations of different disk groups with different colors remain largely unchanged, although the positions of disks in the same color zone are disturbed, and some blocks may change in depth inside the sliding mass (such as disks 22, 25, 31 32) (Fig. 8b). According to Fig. 8b, the deposition area can be divided roughly into three zones, including zone 1 with materials mainly from the upper sliding body, zone 2 with mixed materials from both sliding bodies and zone 3 with materials mainly from the lower sliding body. No obvious boundary exists between different zones. This simulated result is consistent with the field investigation results. Figure 9 shows the differences in the landscape before and after the earthquake. Point a is the position of upper sliding body, point b is the position of undisturbed ground area, and point c is the position of lower sliding body. The upper sliding body is mainly composed of grey-black siliceous phyllite and the lower is composed mainly of yellow unconsolidated sediments. From Fig. 9a, the deposition area can be divided into zones 1, 2 and 3.

5.4 Ejection phenomenon

The simulated results show that the upper sliding face was formed at about 35 s (Fig. 7b) and then the upper sliding body began to move down to gouge out the upper sliding base. When the upper sliding body separated from the upper segment slide face, a free face was formed under the sliding block because of the different dip angle between the upper sliding face and the surface slope. In this stage, some obvious cracks were developing and began to split the sliding body (Fig. 10a). The upper sliding body was then ejected into the air at high velocity. At the same time, the sliding body was destroyed because it developed more cracks (Fig. 10b). Because the ejected body flew through the air, portions of the original ground surface and vegetation remained undisturbed around the zone of ejection; field investigations confirmed the presence of undisturbed ground under the upper sliding body (point b in Fig. 9b). When falling

back to earth, the ejected body disintegrated into debris. At the same time, it began to shovel the lower sliding body, pushing it downwards (Fig. 10c).

5.5 Sliding mechanism of the lower slide body

When the ejected body fell back to earth to shovel and push down the lower sliding body at about 55 s, the formation of the lower segment of the slide face was initiated. Although different sections of the lower sliding body have different velocities, we compare only the displacements of the rear and front parts of the lower sliding body. This is sufficient for describing the sliding mechanism of the lower sliding body. Displacement changes at different locations are shown in Fig. 10. The time intervals were chosen based on the simulation results to illustrate the change of sliding type.

According to Fig. 10, from 55 to 65 s, a ten-meter displacement occurred at the rear part of the lower sliding body. However, no displacement occurred at the toe part of the slide indicating that the lower sliding body began to be shoveled by the falling upper sliding body. The continuous sliding face was not formed at this stage. However, between 65 and 75 s, the displacement, smaller than that at the rear, also occurred at the toe of the slide. The sliding face then probably became continuous and the sliding block moved down along the sliding face. At this stage, the lower landslide became a type of pushed landslide. From 75 to 85 s, both sliding bodies moved down with the same velocity. Afterwards, the landslide changed to the retrogressive type, because the displacement of the toe part was larger than that of the rear part of the landslide. The state between 85 and 95 s (Fig. 11) shows this change.

5.6 Role of erosion processes

Erosion processes also strongly affect the kinematic and runout distances of granular flow on moderate slopes (Mangeney et al., 2007, 2010). They pointed out that the erosion of granular material already present on the bed built up by earlier events can significantly increase the mobility of avalanches flowing on moderate slopes by up to

40 % (Mangeney et al., 2010). In the case of the Donghekou landslide, the influence of eroded beds was only highlighted in the destruction of the original ground surface (Figs. 2 and 4c), which could add eroded material to the landslide as it hurtles down (Fig. 11). We undertook two numerical models, in which the basal erosion model was reproduced based on the model in Fig. 4a. The erosion bed is marked in blue, which was destroyed and slid down when the landslide occurred (Fig. 12). The non-basal erosion model kept this blue part intact, and the landslide material flowed over it (Fig. 12). In the non-basal erosion model, the runout was 1435 m and in the basal erosion model, the runout increased to 1519 m with the additional contribution caused by the destruction of the eroded beds.

6 Conclusions

Based on field studies of the 2008 Donghekou landslide, numerical modeling was conducted to better understand the ejection phenomenon and the formation mechanism of two different sliding faces. The simulated results showed that the large local seismic acceleration and a free face under the sliding body caused by the dip difference between the upper sliding face and the natural slope are responsible for the ejection phenomenon of the landslide. For the lower sliding body, its kinematic mechanism was changed during sliding; it was initially a pushed landslide and then changed to a retrogressive landslide.

This case study indicates that numerical modeling has the potential to bring tight constraints on landslide behavior using information based on available observations and measurements, such as geological and geomorphological conditions, rock mechanics and so on. Two dimensional modeling based on field observations could well explain the kinematic processes of the Donghekou landslide. However, to better explain the geometry of the motion and the lateral spreading of landslide material, three-dimensional modeling should be undertaken in future to better define the features of landslide debris deposits.

Acknowledgements. This study was supported in part by the National Science Council under the grants NSC 97-2116-M-002-022-, 99-2116-M-002-005- and 100-2116-M-002-004-. This study was also supported by Natural Science Foundation of China projects (41172193) and Basic Scientific Funding of Institute of Geology, China Earthquake Administration (IGCEA-1107).

References

Campbell, C. S., Cleary, P. W., and Hopkins, M.: Large-Scale landslide simulations: global deformation velocities and basal friction, J. Geophys. Res., 100, 8267–8283, doi:10.1029/94JB00937, 1995.

Central Geological Survey (Republic of China): Landslide disasters of Taiwan, Geohazard Report, Central Geological Survey, MOEA, Taiwan, Taipei, 2000.

Chigira, M., Wang, W., Furuya, T., and Kamai, T.: Geological causes and geomorphological precursors of the Tsaoling landslide triggered by the 1999 Chi-Chi Earthquake, Taiwan, Eng. Geol., 68, 259–273, doi:10.1016/S0013-7952(02)00232-6, 2003.

Crosta, G. B., Imposimato, S., and Roddeman, D. G.: Continuum numerical modeling of flow-like landslides, in: Landslides from Massive Rock Slope Failure, edited by: Evans, S. G., Mugnozza, G. S., Strom, A., and Hermanns, R. L., Netherlands, Springer, Earth Env. Sci., Vol. 49, 211–232, 2006.

Cruden, D. M. and Varnes, D. J.: Landslide types and processes, in: Landslides Investigation and Mitigation, edited by: Turner, A. K. and Schuster, R. L., National Research Council, Transportation Research Board, Washington DC, 36–75, 1996.

Cundall, P. A.: A computer model for simulating progressive large scale movement in blocky rock systems, Proc. Sym. Int. Soc. Rock. Mech., October 1971, Nancy, France 1, II-8, 1971.

Cundall, P. A. and Strack, P. D. L.: A discrete numerical model for granular assemblies, Geotechnique, 29, 47–65, doi:10.1680/geot.1979.29.1.47, 1979.

Dai, F. C., Xu, C., Yao, X., Xu, L., Tu, X. B., and Gong, Q. M.: Spatial distribution of landslides triggered by the 2008 Ms 8.0 Wenchuan earthquake, China, J. Asian. Earth Sci., 40, 883–895, doi:10.1016/j.jseaes.2010.04.010, 2010

Denlinger, R. P. and Iverson, R. M.: Granular avalanches across irregular three-dimensional terrain: 1. Theory and computation, J. Geophys. Res., 109, F01014, doi:10.1029/2003JF000085, 2004.
Egholm, D. L.: A new strategy for discrete element numerical models: 1. Theory, J. Geophys. Res., 112, B05203, doi:10.1029/2006JB004557, 2007.
Egholm, D. L., Sandiford, M., Clausen, O. R., and Nielsen, S. B.: A new strategy for discrete element numerical models: 2. Sandbox applications, J. Geophys. Res., 112, B05204, doi:10.1029/2006JB004558, 2007.
Harp, E. L. and Jibson, R. W.: Landslides triggered by the 1994 Northridge, California earthquake, B. Seismol. Soc. Am., 86, s319–s332, 1996.
Hu, J.-C. and Angelier, J.: Stress permutations: three-dimensional distinct element analysis accounts for a common phenomenon in brittle tectonics, J. Geophys. Res., 109, B09403, doi:10.1029/2003JB002616, 2004.
Huang, R. and Fan, X.: The landslide story, Nature Geosci., 6, 325–326, doi:10.1038/ngeo1806, 2013.
Huang, R. Q.: Mechanism and geomechanical models of landslide hazards triggered by Wenchuan 8.0 Earthquake, Chinese J. Rock Mech. Eng., 28, 1239–1249, 2009.
Itasca, Consulting Group Inc.: PFC2D Particle Flow Code in 2 Dimensions, User's Guide, Minneapolis, 2002.
Iverson, R. M. and Denlinger, R. P.: Flow of variably fluidized granular masses across three-dimensional terrain, 1. Coulomb mixture theory, J. Geophys. Res., 106, 537–552, doi:10.1029/2000JB900329, 2001.
Iverson, R. M. and Vallance, J. W.: New views of granular mass flows, Geology, 29, 115–118, doi:10.1130/0091-7613(2001)029<0115:NVOGMF>2.0.CO;2, 2001
Keefer, D. K. and Larsen, M. C.: Assessing landslide hazards, Science, 316, 1136–1138, doi:10.1126/science.1143308, 2007.
Keefer, D. K., Wartman, J., Navarro-Ochoa, C., Rodriguez-Marek, A., and Wieczorek, G. F.: Landslides caused by the M 7.6 Tecomán, Mexico earthquake of 21 January 2003, Eng. Geol., 86, 183–197, doi:10.1016/j.enggeo.2006.02.017, 2006.
Legros, F.: The mobility of long-runout landslides, Eng. Geol., 63, 301–331, doi:10.1016/S0013-7952(01)00090-4, 2002.

Li, X., He, S., Lou, Y., and Wu, Y.: Simulation of the sliding process of Donghekou landslide triggered by the Wenchuan earthquake using a distinct element method, Environmental Earth Sciences, 65, 1049–1054, doi:10.1007/s12665-011-0953-8, 2012.
Mangeney, A., Tsimring, L. S., Volfson, D., Aranson, I. S., and Bouchut, F.: Avalanche mobility induced by the presence of an erodible bed and associated entrainment, Geophys. Res. Lett., 34, L22401, doi:10.1029/2007GL031348, 2007.
Mangeney, A., Roche, O., Hungr, O., Mangold, N., Faccanoni, G., and Lucas, A.: Erosion and mobility in granular collapse over sloping beds, J. Geophys. Res.-Earth, 115, F03040, doi:10.1029/2009JF001462, 2010.
Newmark, N. M.: Effect of earthquake on dams and embankments, Geotechnique, 15, 139–160, 1965.
Peng, J. H.: A study on sliding process and depositing behavior in Chiufengershan Landslide, Taipei, Master thesis, National Taiwan University, Taipei, Taiwan, 2008.
Poisel, R. and Roth, W.: Runout models of rock slope failures, Felsbau, 22, 46–50, 2004.
Poisel, R., Bendarik, M., Holzer, R., and Lišč̆ák, P.: Geomechanics of hazardous landslides, J. Mt. Sci., 2, 211–217, 2005.
Potyondy, D. O. and Cundall, P. A.: A bonded-particle model for rock, Int. J. Rock Mech. Min., 41, 1239–1364, 2004.
Sun, P., Yin, Y. P., and Wu, S. R.: Experimental study on shear strength of rocks from Donghekou Landslide in dried state and saturated state, Geol. Bull. China, 28, 1163–1167, 2009a.
Sun, P., Zhang, Y. S., and Yin, Y. P.: Discussion on long runout sliding mechanism of Donghekou landslide-debris flow, Journal of Engineering Geology, 17, 737–744, 2009b.
Staron, L.: Mobility of long-runout rock flows: a discrete numerical investigation, Geophys. J. Int., 172, 455–463, doi:10.1111/j.1365-246X.2007.03631.x, 2007.
Tang, C.-L., Hu, J.-C., Lo, C.-M., and Lin, M.-L.: The catastrophic 1999 Tsaoling and 2009 Hsiaoling klandslides: preliminary study from 3-D distinct element modeling, Sino-Geotec, 122, 143–152, 2009a (in Chinese).
Tang, C.-L., Hu, J.-C., Lin, M.-L., Angelier, J., Lu, C.-Y., Chan, Y.-C., and Chu, H.-T.: The Tsaoling landslide triggered by the CHI-Chi earthquake, Taiwan: insights form a discrete element simulation, Eng. Geol., 106, 1–19, doi:10.1016/j.enggeo.2009.02.011, 2009b.

Tang, C.-L., Hu, J.-C., Lin, M.-L., Yuan, R. M., and Cheng, C.-C.: The mechanism of the 1941 Tsaoling landslide, Taiwan: insight from a 2-D discrete element simulation, Environmental Earth Sciences, 70, 1005–1019, doi:10.1007/s12665-012-2190-1, 2013.

Tang, C.-L., Yuan, R. M., Hu, J.-C., Lin, M.-L., Lee, C.-T., and Liou, Y.-S.: The transportation and deposition of the 2009 Hsiaolin landslide in Taiwan revealed from 3-D granular discrete element simulation, J. Geophys. Res., in revision, 2013.

Tang, H., Jia, H., Hu, X., Li, D., and Xiong, C.: Characteristics of landslide induced by the great Wenchuan earthquake, J. Earth Sci., 21, 104–113, doi:10.1007/s12583-010-0008-1, 2010.

Wang, C., Tannant, D. D., and Lilly, P. A.: Numerical analysis of the stability of heavily jointed rock slopes using PFC2D, Int. J. Rock Mech. Min., 40, 415–424, 2003.

Wang, Y. S., Xu, H. B., Luo, Y. H., and Wu, J. F.: Study of formation conditions and toss motion program of high landslides induced by earthquake, Chinese J. Rock Mech. Eng., 28, 2360–2368, 2009 (in Chinese).

Wilson, R. C. and Keefer, D. K.: Dynamics analysis of a slope failure from the 6 August 1979 Coyote Lake, California, Earthquake, B. Seismol. Soc. Am., 65, 1239–1257, 1983.

Xu, Q. and Dong, X. J.: Genetic types of large-scale landslides induced by Wenchuan Earthquake, Earth Sci. J. China Univ. Geosci., 36, 1134–1142, 2011.

Xu, X. W., Wen, X., Yu, G., Chen, G. H., Klinger, Y., Hubbard, J., and Shaw, J.: Coseismic reverse- and oblique-slip surface faulting generated by the 2008 Mw 7.9 Wenchuan earthquake, China, Geology, 37, 515–518, doi:10.1130/G25462A.1, 2009.

Yin, Y.: Researches on the Geohazards triggered by Wenchuan earthquake, Sichuan, J. Eng. Geol., 16, 1–12, 2008 (in Chinese).

Yin, Y.: Features of landslides triggered by the Wenchuan Earthquake, J. Eng. Geol., 17, 29–38, 2009 (in Chinese).

Yin, Y., Wang, F., and Sun, P.: Landslide hazards triggered by the 2008 Wenchuan earthquake, Sichuan, China, Landslides, 6, 139–152, doi:10.1007/s10346-009-0148-5, 2009.

Yin, Y., Zheng, W., Li, X., Sun, P., and Li, B.: Catastrophic landslides associated with the M8.0 Wenchuan earthquake, B. Eng. Geol. Environ., 70, 15–32, doi:10.1007/s10064-010-0334-7, 2011.

Yoon, J.: Application of experimental design and optimization to PFC model calibration in uniaxial compression simulation, Int. J. Rock Mech. Min., 44, 871–889, doi:10.1016/j.ijrmms.2007.01.004, 2007.

Yuan, R. M., Xu, X. W., Chen, G. H., Tan, X. B., Klinger, Y., and Xing, H. L.: Ejection landslide at northern terminus of Beichuan rupture triggered by 2008 Mw 7.9 Wenchuan earthquake, B. Seismol. Soc. Am., 100, 2689–2699, doi:10.1785/0120090256, 2010.

Yuan, R. M., Deng, Q. H., Cunningham, D., Xu, C., Xu, X. W., Chen, G. H., and Chang, C. P.: Density distribution of landslides triggered by the 2008 Wenchan earthquake and their relationships to peak ground acceleration, B. Seismol. Soc. Am., 103, 2344–2355, doi:10.1785/0120110233, 2013.

Zhang, L. M., Xu, Y., Huang, R. Q., and Chang, D. S.: Particle flow and segregation in a giant landslide event triggered by the 2008 Wenchuan earthquake, Sichuan, China, Nat. Hazards Earth Syst. Sci., 11, 1153–1162, doi:10.5194/nhess-11-1153-2011, 2011.

Zhang, Y., Chen, G., Wu, J., Zheng, L., and Zhuang, X.: Numerical simulation of seismic slope stability analysis based on tension-shear failure mechanism, Geotechnical Engineering Journal of SEAGS-AGSSEA, 43, 18–28, 2012.

Table 1. Micro-properties and macro-properties of models based on a series of biaxial tests.

Parameters of the packing of disks			
Disk density	2650 (kg m^{-3})	Parallel bond modulus (on slope)	50 MPa
Disk thickness	2 (m)	Ball friction coefficient	0.5
Ball-ball contact modulus (landslide block)	5.0 GPa	Parallel bond normal strength parallel to strata (landslide block)	50 MPa
Ball-ball contact modulus (on slope)	50 MPa	Parallel bond normal strength non-parallel to strata (landslide block)	10 Mpa
Ball stiffness ratio	1	Parallel bond shear strength parallel to strata (landslide block)	50 MPa
Minimum ball radius (Rmin)	0.64 m	Parallel bond shear strength non-parallel to strata (landslide block)	10 Mpa
Ball size ratio (Rmax/Rmin)	2.0	Parallel bond normal strength (on slope)	1 MPa
Parallel bond radius multiplier	1	Parallel bond shear strength (on slope)	1 MPa

Table 2. Runout distance of the monitoring disks in the landslide blocks.

	Disk No.	Runout distance, m	Disk No.	Runout distance, m	Disk No.	Runout distance, m	Disk No.	Runout distance, m
Upper disks	3	1079	21	1730	32	1802	40	1358
Lower disks	4	1263	22	1304	30	1548	39	1069

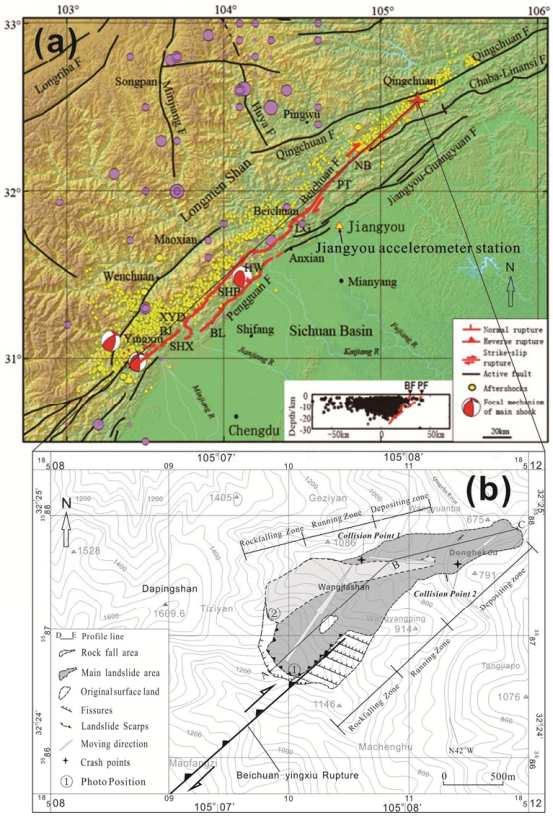

Fig. 1. Main shock and aftershocks of the Wenchuan earthquake, regional structures, and outline of the Donghekou landslide.

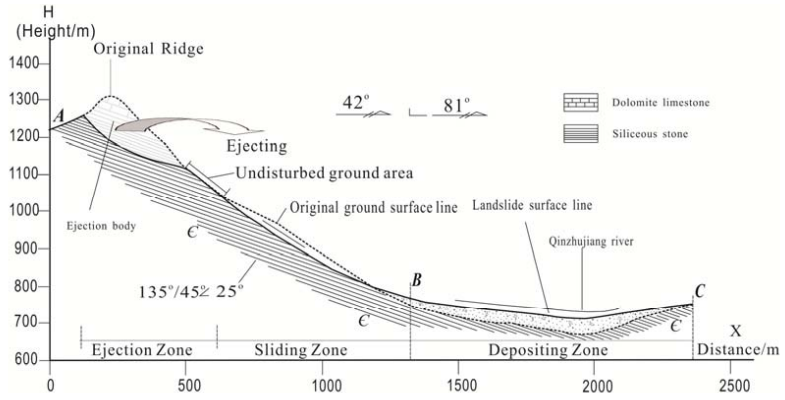

Fig. 2. A geologic profile (A-B-C) of the Donghekou landslide (Yuan et al., 2010; profile shown in Fig. 1).

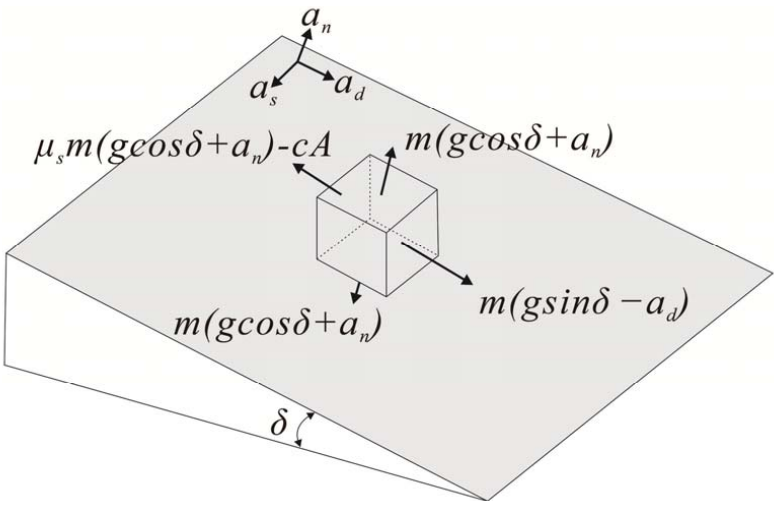

Fig. 3. Diagram illustrating the critical balance condition of forces exerted on a rock block lying on an inclined planar surface under the earthquake ground motion.

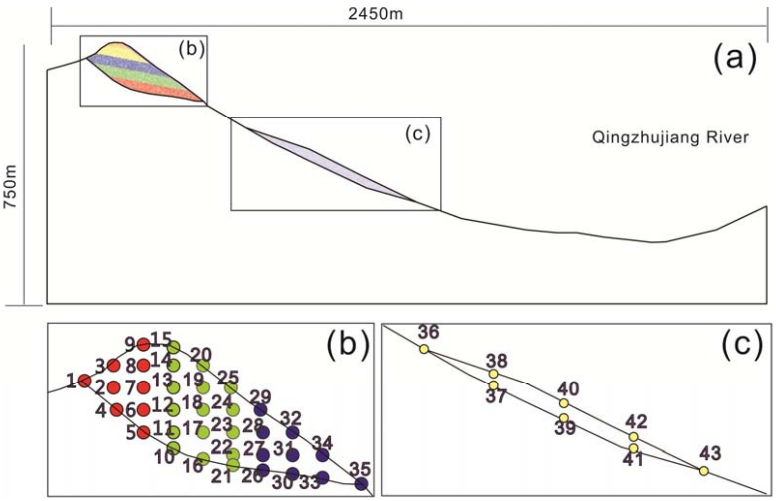

Fig. 4. Numerical model of the Donghekou landslide and the monitoring disks within the sliding blocks.

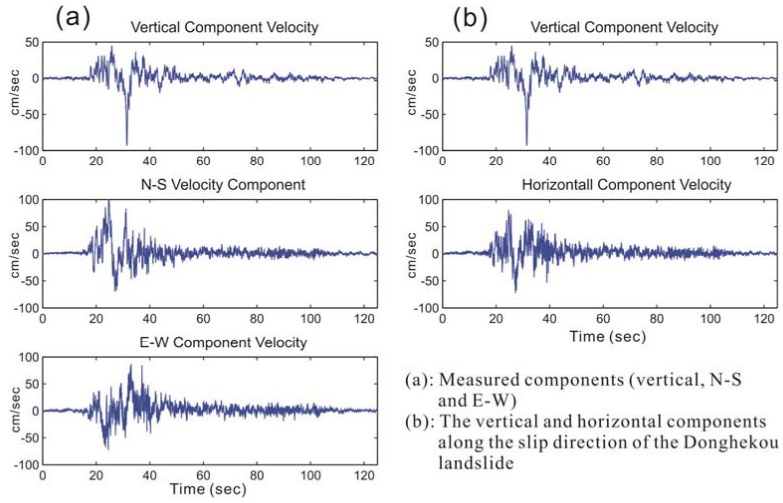

Fig. 5. Velocity diagram of the accelerometer station in Jiangyou during the Wenchuan earthquake.

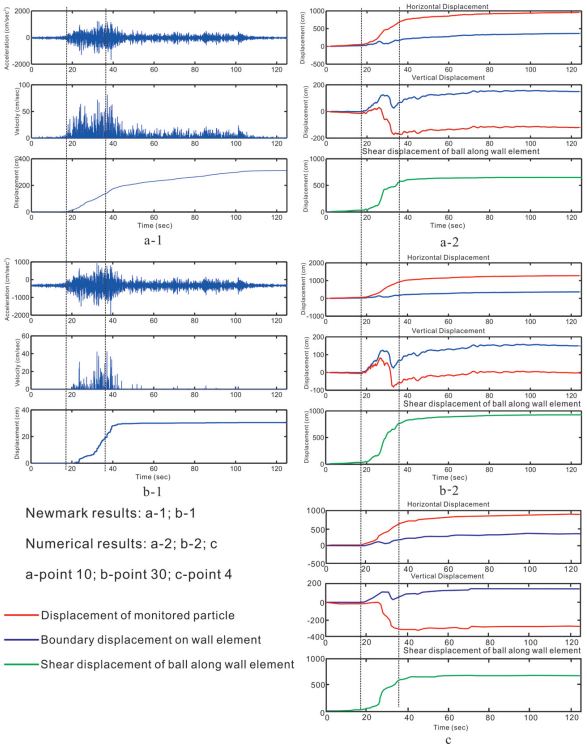

Fig. 6. Acceleration and displacement under shaking based on Newmark and numerical methods (the red and blue lines in the right column of Fig. 6 are the displacements of the monitored particles and boundary displacements, respectively. Positions of the disks shown in Fig. 4.).

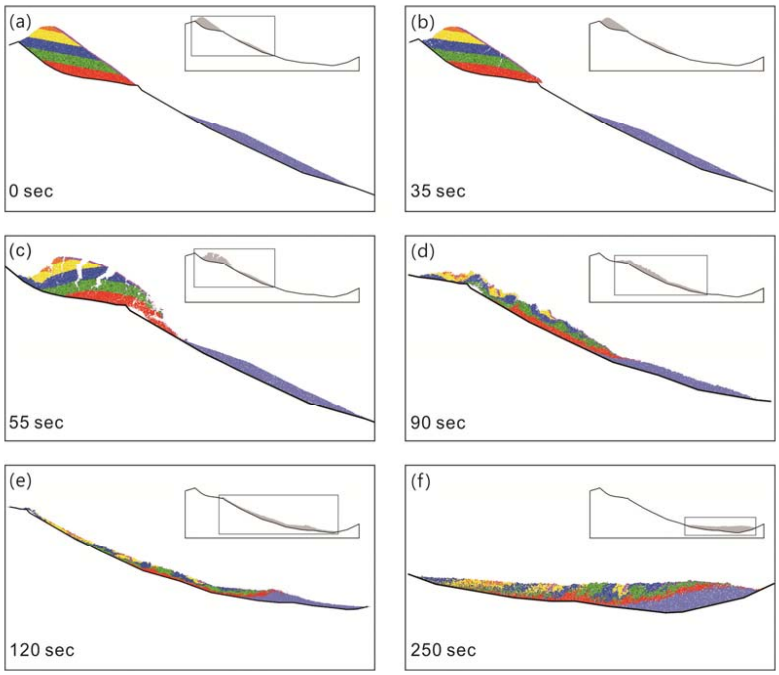

Fig. 7. Simulated results of the Donghekou landslide at different time stages.

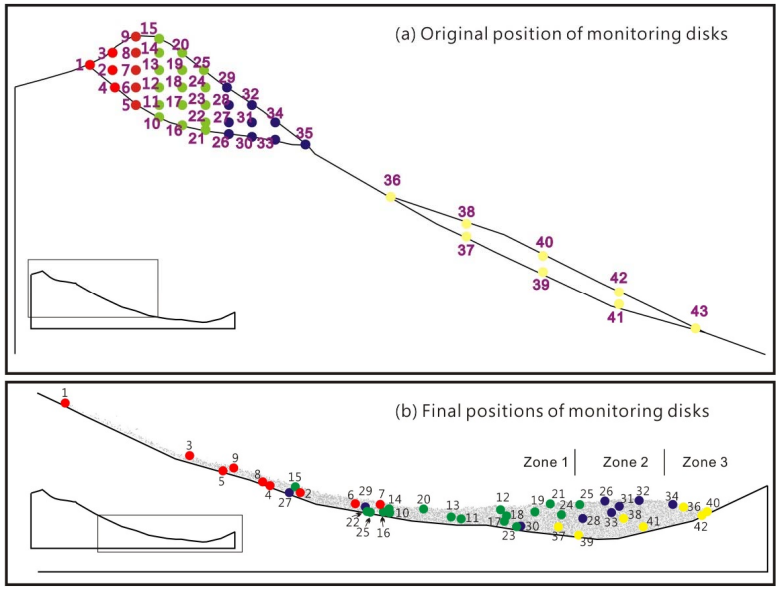

Fig. 8. Comparison between original and final positions of monitoring disks.

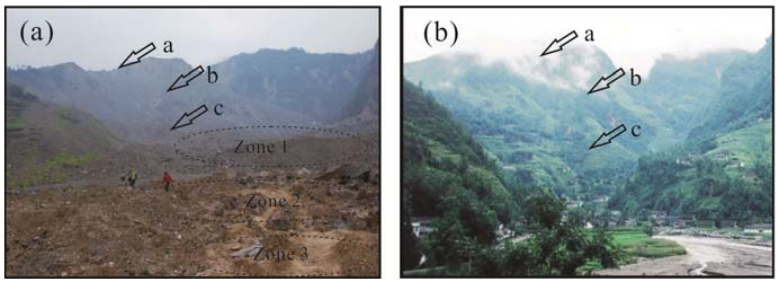

Fig. 9. Pictures of the landslide after **(a)** and before **(b)** the earthquake (view looking to the southwest).

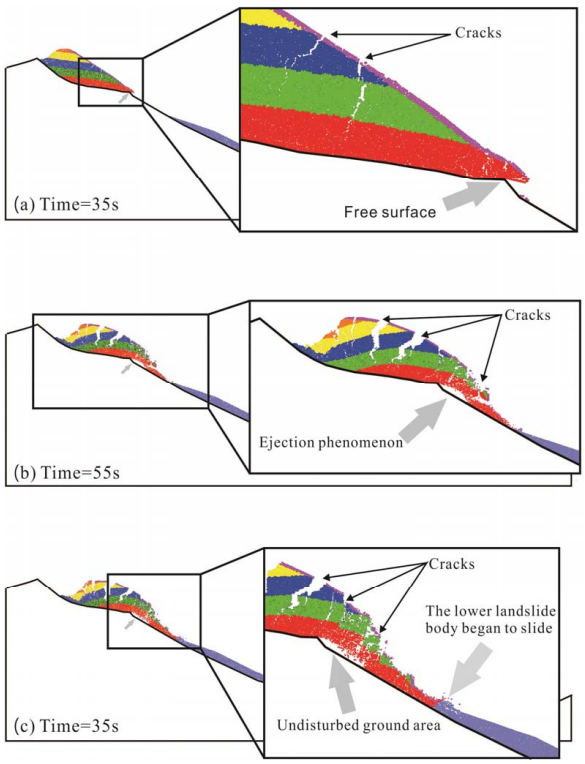

Fig. 10. Ejection phenomenon in the Donghekou landslide.

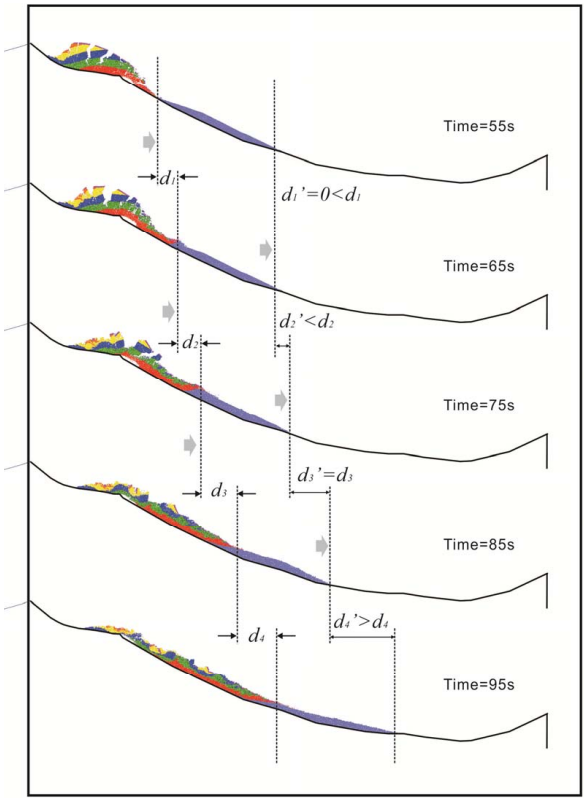

Fig. 11. Displacement changes in different parts of the lower landslide body.

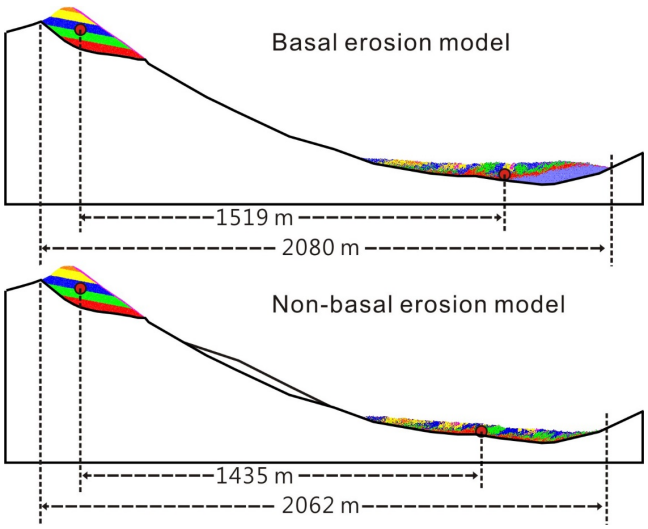

Fig. 12. Runout of basal erosion model and non-basal erosion model.